

Enhancement of AC System Stability using Artificial Neural Network Based HVDC Controls

Nagu. B*, Ramana Rao P.V.*, Sydulu M.*

* National Institute of Technology-Warangal/Dept. of Electrical Engineering, Warangal, India.

Article Info

Article history:

Received Mar 5, 2013
Revised May 25, 2013
Accepted Jun 27, 2013

Keyword:

HVDC,
Transient stability,
Multi-machine
stability,
NN based controller.

ABSTRACT

In this paper, investigation is carried out for the improvement of power system stability by utilizing auxiliary controls for controlling HVDC power flow. The current controller model and the line dynamics are considered in the stability analysis. Transient stability analysis is done on a multi-machine system, where, a neural network controller is developed to improve the stability of the power system and to improve the response time of the controller to the changing conditions in power system. The results show the application of the neural network controller in AC-DC power systems and case studied at different fault locations.

Copyright © 2013 Institute of Advanced Engineering and Science.
All rights reserved.

Corresponding Author:

Nagu. B
Department of Electrical Engineering,
National Institute of Technology- Warangal-506004,
Email Id : nagu.research@gmail.com

1. INTRODUCTION

HVDC power transmission system offers several advantages, one of which is to rapidly control the transmitted power. Therefore, they have a significant impact on the stability of the associated AC power systems. Moreover, HVDC link is effective for frequency control and improves the stability of the system using fast load-flow control. The importance of AC-DC power transmission systems regarding improvement of stability has been a subject to much research. An HVDC transmission link is highly controllable. It is possible to take advantage of this unique characteristic of the HVDC link to augment the transient stability of the ac systems.

A proper design of the HVDC controls is essential to ensure satisfactory performance of overall AC/DC system [1]. The control strategy traditionally employed for a two-terminal HVDC transmission system is the current margin method, whereby the rectifier is in current control, and the inverter is in constant extinction angle (CEA) control [2]. Both ends of the dc system rely on PI controllers to provide fast robust control. Such controllers, however, suffer from the following disadvantages:

- Control parameters are optimal only over a limited range,
- A prior knowledge of system dynamics is required to optimize the controllers,

Microprocessor based adaptive controllers are increasingly being used within the industry to adapt controller parameters as function of operating angle, system topology, and prior knowledge of system dynamics.

Also, the Artificial Neural Network (ANN) based controller can be used satisfactorily to control the power flow through HVDC line.

In this paper, it is explored that how NN based controller can be optimal over wide range and how they are better in performance and fast in response.

With NN-based controllers the following advantages are possible:

- Optimal control over a wide range,
- They have capability to learn from previous experience.

In this paper, the feasibility of employing a NN-based controller for an HVDC transmission system is explored.

2. AC/DC LOAD FLOW ANALYSIS

In transient stability studies it is a prerequisite to do AC/DC load flow calculations in order to obtain system conditions prior to the disturbance. While the conventional approaches are available for conducting the calculations, the eliminated variable method is used here which treats the real and reactive powers consumed by the converters as voltage dependent loads. The dc equations are solved analytically or numerically and the dc variables are eliminated from the power flow equations. The method is however unified in the sense that the effect of the dc-link is included in the Jacobian. It is, however, not an extended variable method, since no dc variables are added to the solution vector.

2.1. DC System Model

The single line diagram and equivalent circuit of monopolar DC link are shown in the following figures.



Figure 1. Monopolar HVDC link

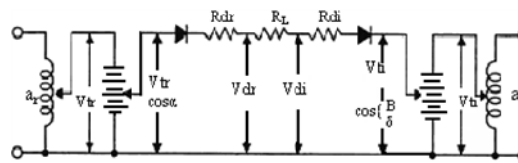


Figure 2. Equivalent circuit of monopolar HVDC link

The equations describing the steady state behavior of a monopolar DC link can be summarized as follows.

$$V_{dr} = \frac{3\sqrt{2}}{\pi} a_r V_{tr} \cos \alpha_r - \frac{3}{\pi} X_c I_d \tag{2.1}$$

$$V_{dt} = \frac{3\sqrt{2}}{\pi} a_t V_{tt} \cos \gamma_t - \frac{3}{\pi} X_c I_d \tag{2.2}$$

$$V_{dr} = V_{dt} + r_d I_d \tag{2.3}$$

$$P_{dr} = V_{dr} I_d \tag{2.4}$$

$$P_{dt} = V_{dt} I_d \tag{2.5}$$

$$S_{dr} = k \frac{3\sqrt{2}}{\pi} a_r V_{tr} I_d \tag{2.6}$$

$$S_{dt} = k \frac{3\sqrt{2}}{\pi} a_t V_{tt} I_d \tag{2.7}$$

$$Q_{dr} = \sqrt{S_{dr}^2 - P_{dr}^2} \quad (2.8)$$

$$Q_{di} = \sqrt{S_{di}^2 - P_{di}^2} \quad (2.9)$$

Where,

| | |
|-----------------------------------|---|
| V _{dr} , V _{di} | voltages at rectifier and inverter end respectively, |
| V _{tr} , V _{ti} | terminal voltages at rectifier and inverter ends, |
| I _d | dc link current, |
| X _c , r _d | dc link reactance and resistance, |
| α, γ | firing and extinction angle respectively, |
| a | tap ratio, |
| P _{dr} , P _{di} | Real power at rectifier and inverter ends respectively, |
| Q _{dr} , Q _{di} | Reactive power at rectifier and inverter ends respectively, |
| S _{dr} , S _{di} | Apparent power at rectifier and inverter ends respectively [3]. |

2.2. Eliminated Variable Method

The real and reactive powers consumed by the converters can then be written as functions of their ac terminal voltages, V_{tr} and V_{ti}. It is not needed to derive explicit functions for the real and reactive powers, only to find a sequence of computations such that the real and reactive powers and their partial derivatives w.r.t. the AC terminal voltages can be computed.

$$\begin{bmatrix} \Delta P \\ \Delta Q \end{bmatrix} = \begin{bmatrix} H & N \\ J & L \end{bmatrix} \begin{bmatrix} \Delta \delta \\ \Delta V/V \end{bmatrix} \quad (2.10)$$

$$N^r(tr, tr) = V_{tr} \frac{\partial P_{tr}^{\alpha\gamma}}{\partial V_{tr}} + V_{tr} \frac{\partial P_{dr}(V_{tr}, V_{ti})}{\partial V_{tr}} \quad (2.11)$$

$$N^r(tr, ti) = V_{ti} \frac{\partial P_{tr}^{\alpha\gamma}}{\partial V_{ti}} + V_{ti} \frac{\partial P_{dr}(V_{tr}, V_{ti})}{\partial V_{ti}} \quad (2.12)$$

$$N^i(ti, tr) = V_{tr} \frac{\partial P_{tr}^{\alpha\gamma}}{\partial V_{tr}} - V_{tr} \frac{\partial P_{di}(V_{tr}, V_{ti})}{\partial V_{tr}} \quad (2.13)$$

$$N^i(ti, ti) = V_{ti} \frac{\partial P_{tr}^{\alpha\gamma}}{\partial V_{tr}} - V_{ti} \frac{\partial P_{di}(V_{tr}, V_{ti})}{\partial V_{ti}} \quad (2.14)$$

L' is modified analogously [3]. Thus, in the eliminated variable method, four mismatch equations and up to eight elements of the Jacobian have to be modified, but no new variables are added to the solution vector, when a DC-link is included in the power flow.

2.3. Generator Representation

The synchronous machine is represented by a voltage source, in back of a transient reactance, that is constant in magnitude but changes in angular position neglecting the effect of saliency and assumes constant flux linkages and a small change in speed.

$$\frac{d\delta}{dt} = \omega - 2\pi f \quad (2.15)$$

$$\frac{d^2\delta}{dt^2} = \frac{d\omega}{dt} = \frac{\pi f}{H(P_m - P_e)} \quad (2.16)$$

$$E^* = E_c + I_t r_a + jx_d' I_t \quad (2.17)$$

Where

| | |
|------------------|-------------------------------------|
| E' | Voltage back of transient reactance |
| E_t | Machine terminal voltage |
| I_t | Machine terminal current |
| r_a | Armature resistance |
| x_d | Transient reactance |
| δ, ω | Rotor angle and Speed respectively |
| P_m, P_e | Mechanical and Electrical Power |
| H | Inertia constant |

2.4. Load representation

The static admittance Y_{p0} used to represent the load at bus P, can be obtained from,

$$Y_{p0} = \frac{I_{p0}}{E_p} \quad (2.18)$$

$$I_{p0} = \frac{P_{lp} - Q_{lp}}{E_p^2} \quad (2.19)$$

Where,

| | |
|----------|--|
| I_{p0} | Current flows from p^{th} bus to ground |
| E_p | Calculated bus voltages at p^{th} bus |
| P_{lp} | Scheduled active load at p^{th} bus |
| Q_{lp} | Scheduled reactive load at p^{th} bus |

2.5. HVDC representation

Each DC system tends to have unique characteristics tailored to meet the specific needs of its application. Therefore, standard models of fixed structures have not been developed for representation of DC systems in stability studies. The current controller employed here (figure 3(a)) is a proportional integral controller and the auxiliary controller is taken to be a constant gain controller.

HVDC line is represented using transfer function model [4] as shown in the figure 3(b).

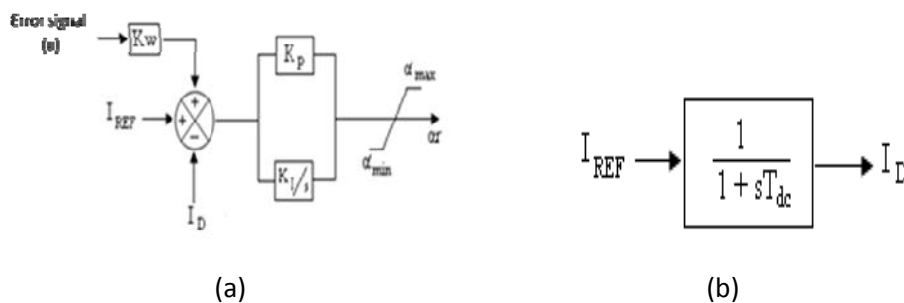


Figure 3. (a) Current controller and auxiliary controller (b) Transfer function model.

2.6. Steps for AC/DC Transient Stability Study

The basic structure of transient stability program is given below [5]:

- 1) The initial bus voltages are obtained from the AC/DC load flow solution prior to the disturbance.
- 2) After the AC/DC load flow solution is obtained, the machine currents and voltages behind transient reactance are calculated.
- 3) The initial speed is equated to $2\pi f$ and the initial mechanical power is equated to the real power output of each machine prior to the disturbance.
- 4) The network data is modified for the new representation. Extra nodes are added to represent the generator internal voltages. Admittance matrix is modified to incorporate the load representation.
- 5) Set time, $t=0$;

- 6) If there is any switching operation or change in fault condition, modify network data accordingly and run the AC/DC load flow.
- 7) Using Runge-Kutta method, solve the machine differential equations to find the changes in the internal voltage angle and machine speeds.
- 8) Internal voltage angles and machine speeds are updated and are stored for plotting.
- 9) Advance time, $t=t+\Delta t$.
- 10) Check for time limit, if $t \leq t_{max}$ repeat the process from step 6, else plot the graphs of internal voltage angle variations and stop the process.

Basing on the plots, that we get from the above procedure it can be decided whether the system is stable or unstable.

In case of multi machine system stability analysis the plot of relative angles is done to evaluate the stability.

3. CONVENTIONAL CONTROLLER

A WSCC-9 system is taken for stability analysis. It is given in the figure 4. A fault is assumed to occur on Line 4-6, at initial time zero. It is assumed that a grounded fault occurred near to Bus 6 and the line from Bus 4 to Bus 6 is removed after 4 cycles. The HVDC line is located between buses 4 –5. Under these conditions, the impact of HVDC on system stability is presented. Initially, a case in which the HVDC line maintains the same control as in the normal state, in which the post-fault HVDC power flow setting remains the same as before, is investigated. It was found that, the system becomes unstable. Then a controller is designed to stabilize the system.

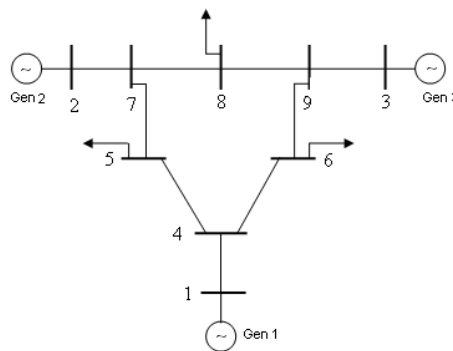


Figure 4. WSCC 9 Bus System

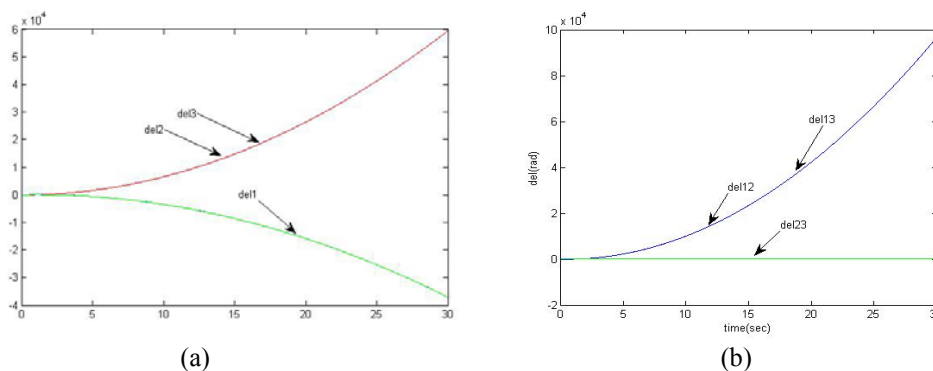


Figure 5. (a) Plot of absolute angles without controller (b) plot of relative angles without controller when HVDC at 4-5 & fault at 4-6

It is clearly seen in figure 5(a) that the system is becoming unstable, generator 2 and generator 3 are moving together whereas generator 1 falling out of synchronism, with this group. To stabilize the system, it is necessary to make equal accelerations of all the generators. So an error signal representing average difference in accelerations of the generators is considered. In case of multi machine system, the relative angles are to be

maintained within limits to maintain the stability of the system. So, error signals derived from the average difference in the relative angles and average difference in the relative speeds of the generators are considered. These error signals are shown below.

$$error_1 = \left[\left(\frac{\omega(2) - \omega(1) + \omega(3) - \omega(1)}{2} \right) - (\omega(2) - \omega(3)) \right] \quad (3.1)$$

$$error_2 = \left[\left(\frac{del(2) - del(1) + del(3) - del(1)}{2} \right) - (del(2) - del(3)) \right] \quad (3.2)$$

$$error_3 = \left[\left(\frac{\frac{P_{mis}(3)}{H(3)} + \frac{P_{mis}(2)}{H(2)}}{2} \right) - \left(\frac{P_{mis}(1)}{H(1)} \right) \right] \quad (3.3)$$

Where,

- $\omega(i)$ Instantaneous Speed of generator i , for $i=1,2,3$.
- $del(i)$ Rotor angle of generator i , for $i=1,2,3$.
- $P_{mis}(i)$ Acceleration in rotor of generator i , for $i=1,2,3$.
- $Error_1$ Average difference in the relative speeds of the three generators
- $Error_2$ Average difference in the relative angles of the three generators
- $Error_3$ Average difference in the relative accelerations of the three generators

Different combinations of the above three signals are considered, in order to improve the stability. Gains of the signals are varied in order to get better transient and dynamic performance.

When $error_1$ signal alone is considered for improving the stability of the system as suggested [6], the plot of relative angles is shown in Figure 6 which reveals that the considered signal is inadequate to improve the stability of the system.

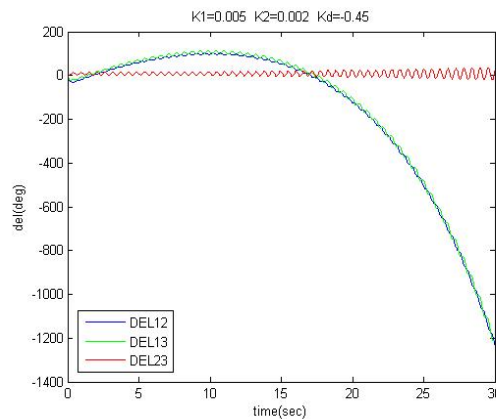


Figure 6. Plot of relative angles with $error_1$ as the control signal (P-controller)

When considering the combination of $error_1$ and $error_2$ signals the control signal is generated, and the PI-Controller is implemented to control the HVDC link and the plot of relative angles is shown below. When HVDC link is 4-5 and fault is in line 4-6. The plot of relative angles deviation and plot of absolute angles are shown in the figure 7(a) and figure 7(b) respectively.

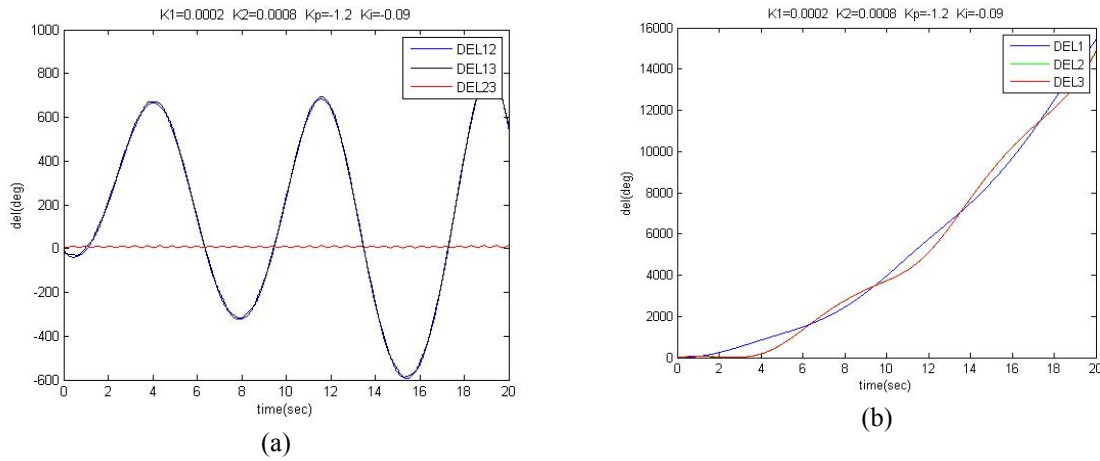


Figure 7. (a)Relative generator angles with PI-controller (b) Absolute generator angles with PI-controller

Considering the combination of error₁, error₂ and error₃ signals to generate the control signals, and it was found that by considering all the three signals the stability of the system is improved. The signal error₂ is the equivalent to the integral of the signal error₁ and the signal error₃ is equivalent to the differential of the signal error₁. Hence, the controller is equivalent to PID controller [7]. The plot of relative angles with error1, error2 and error3 as control signals is shown in figure 8(a) and the plot of the absolute angles is also shown in the figure 8(b).

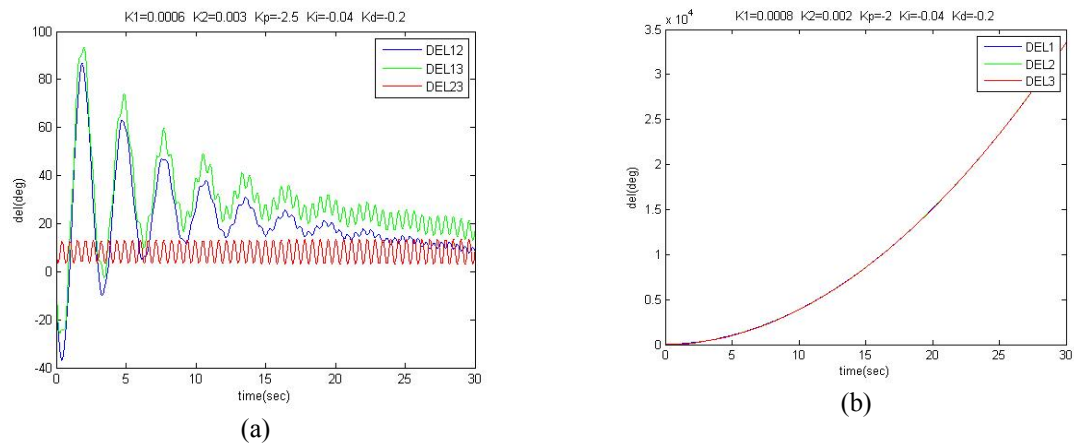


Figure 8. Plot of(a) Relative angles with PID controller (b) Absolute angles with PID controller when HVDC at 4-5 & fault at 4-6

From above simulations it is clearly shown that among all controllers (i.e. P, PI, PID) PID controller has the best result.

Then the control signal can be equivalently represented in the following equation

$$Error = K_p e(t) + K_i \int e(t) dt + K_d \frac{de(t)}{dt} \tag{3.4}$$

$$Error = K_p * error1 + K_i * error2 + K_d * error3 \tag{3.5}$$

Where,

K_p = proportional constant,

K_i = integral constant,

K_d = differential constant.

Case II The response of PID controller when HVDC at 4-5 and fault at line 8-9

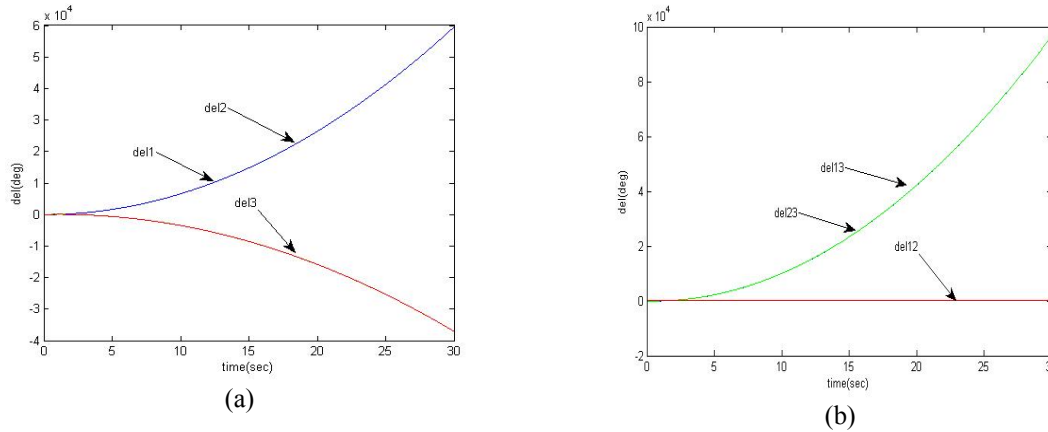


Figure 9. Plot of (a) absolute angles without cotroller (b) Relative angles without cotroller when HVDC at 4-5 & fault at 8-9

It is clearly seen in figure 9(a) that the system is becoming unstable, generator 2 and generator 3 are moving together whereas generator 1 falling out of synchronism, with this group. To stabilize the system, it is necessary to make equal accelerations of all the generators. So an error signal representing average difference in accelerations of the generators is considered. In case of multi machine system, the relative angles are to be maintained within limits to maintain the stability of the system. So, error signals derived from the average difference in the relative angles and average difference in the relative speeds of the generators are considered. These error signals are shown below.

$$error_1 = \left[\left(\frac{\omega(2) - \omega(3) + \omega(1) - \omega(3)}{2} \right) - (\omega(2) - \omega(1)) \right] \tag{3.6}$$

$$error_2 = \left[\left(\frac{del(2) - del(3) + del(1) - del(3)}{2} \right) - (del(2) - del(1)) \right] \tag{3.7}$$

$$error_3 = \left[\left(\frac{\frac{P_{mts(1)}}{H(1)} + \frac{P_{mts(2)}}{H(2)}}{2} \right) - \left(\frac{P_{mts(3)}}{H(3)} \right) \right] \tag{3.8}$$

Since, PID controller is best among all conventional controllers, therefore, for this case we will consider the response of PID controller only. In the second case when HVDC line at 4-5 and fault occurs at line 8-9 then the responses of relative angles are shown in the figure10(a) and the response of absolute angles are also shown in figure 10(b).

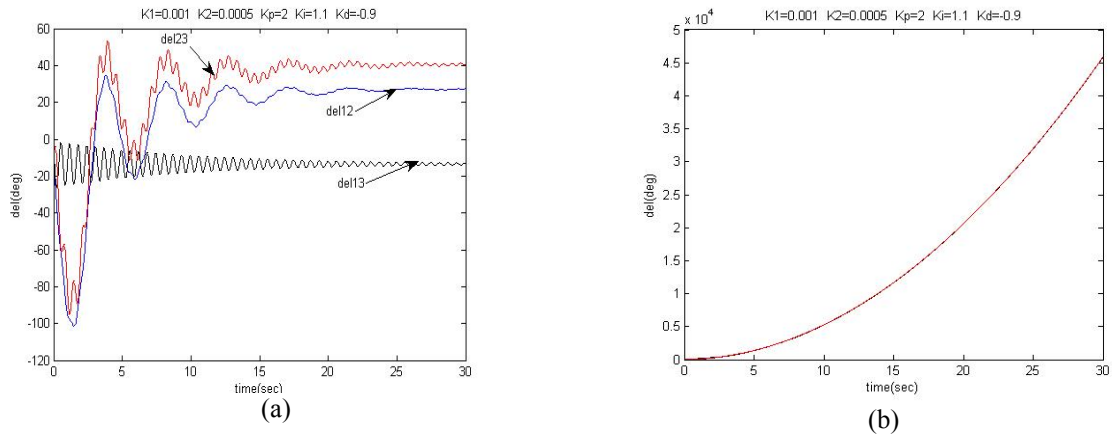


Figure 10. Plot of (a) Relative angles with PID controller (b) Absolute angles PID controller when HVDC at 4-5 & fault at 8-9

4. ANN FEED FORWARD OFF-LINE CONTROLLER

HVDC systems traditionally use PI controllers with fixed gains. Although such controllers have certain disadvantages, they are rugged and operate satisfactorily for perturbation within a small operating range.

4.1. Development of NN-based Controller

The structure of the NN-based controller is shown in Figure 11. The controller is trained off-line to obtain values of weights that make the error, approach zero. The NN consists of the following three layers.

- 1) **Input Layer:** In this layer there are only two neurons, one of which is fed from a constant input bias, BIAS2. The input to other neuron is error. This layer acts simply as a fan-out layer, and hence the outputs of the neurons are BIAS2 and error.
- 2) **Hidden Layer:** In this layer there are $N = 5$ neurons. These are connected to the outputs of input layer by weights X_n and BB_n , where $n = 1, 2, \dots, N$. The outputs of these neurons are acted upon by the sigmoid function. The 5 neuron outputs in the hidden layer are fed to the output layer through the weights Y_n .
- 3) **Output Layer:** This layer consists of one neuron only. The inputs to this neuron are the outputs O_n from the hidden layer and BIAS2 from input layer. The weights associated with these inputs are Y_n and BB , respectively. The output of this layer is OUT2, which is fed to a scaling factor π .

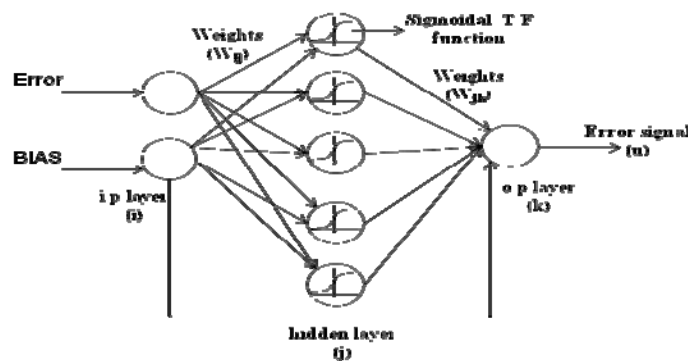


Figure 11. NN-Based Controller Model

A. Training the Off-Line NN

Figure 12 shows the method for training the off line trained NN by copying an existing PI controller [8].

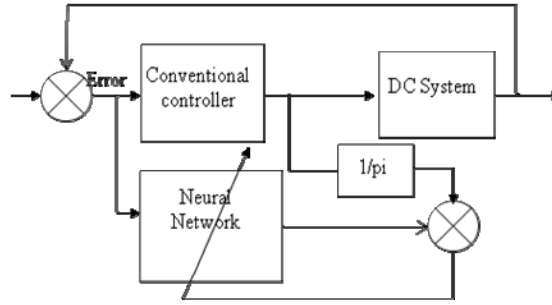


Figure 12. Block Diagram of DC system with NN-based controller

The existing PI controller does not need to be well optimized, as long as the overall system is stable [9]. The input to the NN is error1 or error2 or error3 or combination of any two or combination of all three errors corresponding to P, I, D, PI, PD, PID controller and output is OUT2. The errors are obtained from existing DC system model with conventional controller. The error α_c between the target alpha T (obtained from conventional controller i.e. PI, PD, PID controllers) and the OUT2 is used to adjust the weights of NN according to generalized delta rule. The target $T = \alpha_c/\pi$, and the error to be minimized during training is,

$$\alpha_c = 0.5 * (T - OUT2)^2 \tag{4.1}$$

The training patterns are nothing but the set of error1 or error2 or error3 or combination of any two or combination of all three depending upon the controller used (P,I,D,PI,PD,PID). This set is obtained from conventional controller by taking instantaneous values of errors i.e. error1, error2, or error3.

In this paper, for the given system, 6000 patterns have taken for training and testing the NN. These patterns (error1, error2, error3etc.) are obtained from conventional controller. Out of 6000, 20% patterns (i.e.1200) have taken for testing and remaining for training purpose. The corresponding output is taken as the target output (T).

The training of the off-line controller is difficult to achieve with an actual system; therefore, learning from existing controllers used with simulators seems to be the logical choice at present. Alternative methods for training are feasible [10].

B. Adjusting the Weights in the Output Layer

Using the delta rule at the output, δ is defined as

$$\delta = \left(\frac{dOUT2}{dNET2} \right) * (T - OUT2) \tag{4.2}$$

Where, $OUT2 = \frac{1}{1 + e^{-NET2}}$

$$NET2 = BB * BIAS2 + \sum_{n=1}^N Y_n * O_n$$

Hence,

$$\delta = OUT2 * (1 - OUT2) * (T - OUT2) \tag{4.3}$$

Then the modifications in the weights are given by,

$$\Delta Y_n(t + 1) = \eta * \delta * O_n + \mu * \Delta Y_n(t) \tag{4.4}$$

$$\Delta BB_n(t + 1) = \eta * \delta * BIAS2 + \mu * \Delta BB_n(t) \tag{4.5}$$

Therefore, the updated values of weights Y_n and BB are,

$$Y_n(t+1) = \Delta Y_n(t) + \Delta Y_n(t+1) \quad (4.6)$$

$$BB_n(t+1) = \Delta BB_n(t) + \Delta BB_n(t+1) \quad (4.7)$$

C. Adjusting the Weights in the Hidden Layer

Now the error is back-propagated through the weights Y_n of the output layer to adjust the weights X_n and BB_n of the hidden layer. Using the sigmoid function, the outputs from the hidden layer are,

$$O_n = \frac{1}{1 + e^{-NET_1}} \quad (4.8)$$

Where,

$$NET_{1n} = X_n * \text{error} + BB_n * \text{BIAS2}$$

Now, using the delta rule,

$$\delta_n = Y_n * \delta * \left(\frac{dO_n}{dNET_{1n}} \right)$$

$$\delta_n = Y_n * \delta * O_n * (1 - O_n) \quad (4.9)$$

Then the modifications in the weights are,

$$\Delta X_n(t+1) = \eta * \delta * \sigma + \mu * \Delta X_n(t)$$

$$\Delta BB_n(t+1) = \eta * \delta * \text{BIAS2} + \mu * \Delta BB_n(t)$$

Hence, the updated values of the weights X_n and BB_n are,

$$X_n(t+1) = \Delta X_n(t) + \Delta X_n(t+1)$$

$$BB_n(t+1) = \Delta BB_n(t) + \Delta BB_n(t+1)$$

The problem with off-line training is the uncertainty of the parameters of ac/dc system, which are only approximately known (at best). Moreover, these parameters vary from time to time. This means that the parameters preset for either the traditional PP or off-line trained NN may not be optimal for all times and operating conditions. However, the advantage of the off-line trained controller (once it has been trained) is its capacity to generalize and its superior speed of response.

4.2. Testing of NN based Controller

To test the effectiveness of the above controllers the HVDC system is subjected to a Three-phase-to-ground fault at the converter end AC bus. Variation of dc link voltage and current, and converter firing angle due to a three-phase-to-ground fault at the rectifier end AC bus. The dc bus voltage completely collapses and results in commutation failure of the converter thyristors. During the fault, the DC link current drops to zero and the firing angle settles at the minimum value. The zero current and zero power condition lead to complete de-energization of the DC link. As soon as the fault is cleared the converter current controller gets activated, and it is in this period when the performance is influenced by the controller actions. The implementation of NN-based controllers is also less complicated than that of sophisticated identification and optimization procedures.

However, Testing of NN is done by using updated weights which are obtained from Training.

4.3. Application of ANN (Neural Network)-based Controller to WSCC 9 Bus System

The above mentioned NN-based Controller is used for the WSCC 9 bus system. The NN-based PID Controller are applied to the WSCC 9 bus system and the simulations are generated and are shown below. The off-line NN controller has a fast response; it is unable to match completely the transient response as obtained from conventional controller. This is a result of the limited training set utilized; actually, it is very difficult to train the off-line NN for all operating conditions.

However, the fast response and better performance overcome many of the disadvantages of conventional controller.

4.3.1. The NN-based P (Proportional) Controller

Case I: when HVDC at 4-5 and fault at 4-6

Similar to conventional P controller error is given as input to input layer of NN figure 13(a) and alpha is determined. A graph of relative angles δ_{23} , δ_{13} & δ_{12} is plotted in figure 13(b).

The relative angle δ_{23} has remained constant as usual. Though the fault is cleared, the relative angles δ_{13} & δ_{12} goes unsynchronized. Due to this controller these relative angles δ_{13} & δ_{12} has reached the steady state at about 18 seconds.

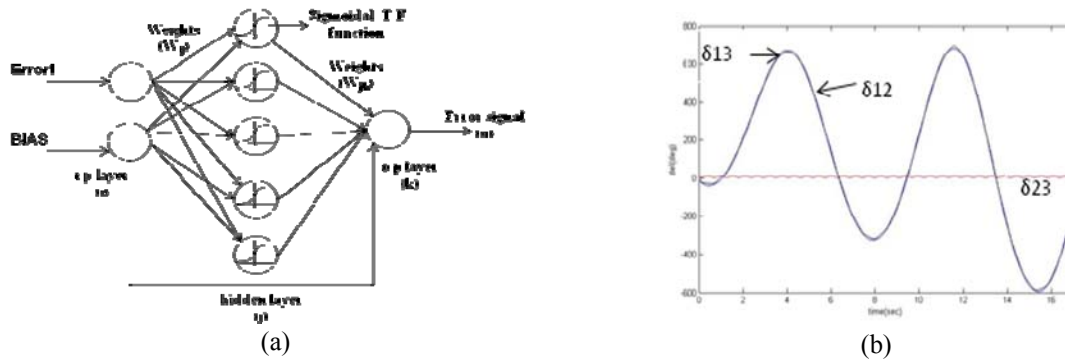


Figure 13. (a) NN based P-controller (b) Plot of relative angles with ANN based P-controller

4.3.2. The NN-based P-I (Proportional-Integral) Controller

Case I: when HVDC at 4-5 and fault at 4-6

Similar to conventional PI controller error1 and error3 is given as input to input layer of NN figure 14(a) and alpha is determined. A graph of relative angles δ_{23} , δ_{13} & δ_{12} is plotted as shown in figure 14(b).

The relative angle δ_{23} has remained constant as usual. Though the fault is cleared, the relative angles δ_{13} & δ_{12} goes unsynchronized. Due to this controller these relative angles δ_{13} & δ_{12} has reached the steady state at about 16 seconds.

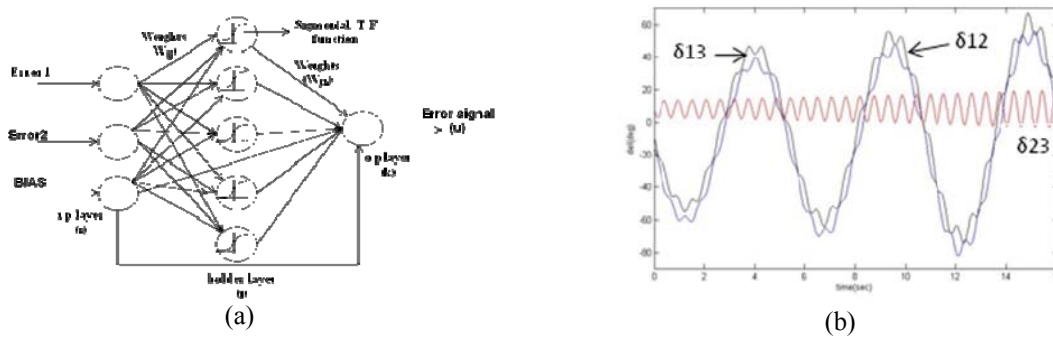


Figure 14. (a) ANN based P-I controller (b) Plot of relative angles with ANN based P-I controller

4.3.3. The NN-based PID (Proportional-Integral-Differential) Controller

Case I: when HVDC at 4-5 and fault at 4-6

Similar to conventional PID controller error1, error2 and error3 is given as input to input layer of NN in figure 15 and alpha is determined. A graph of relative angles δ_{23} , δ_{13} & δ_{12} is plotted in figure 24. It is clearly observed that the generator-1 tries to go out of synchronism when the fault occurs on the line 4-6 near bus-6. but it is brought back in synchronism with the generator-2 and generator-3 with the help of ANN based PID-Control of HVDC link 4-5. Due to this controller these relative angles δ_{13} & δ_{12} has reached the steady state at about 12 seconds. the plot of relative angles and absolute angles are shown in figure 16(a) and figure 16(b) respectively.

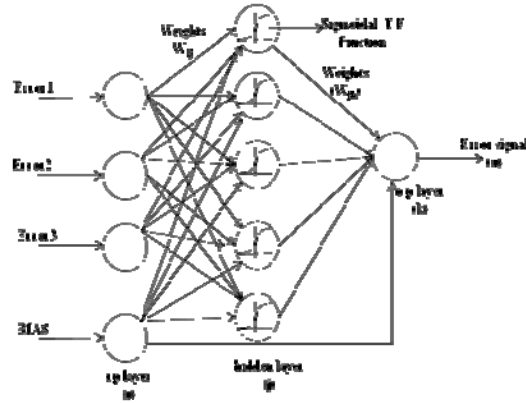


Figure 15. ANN based PID Controller

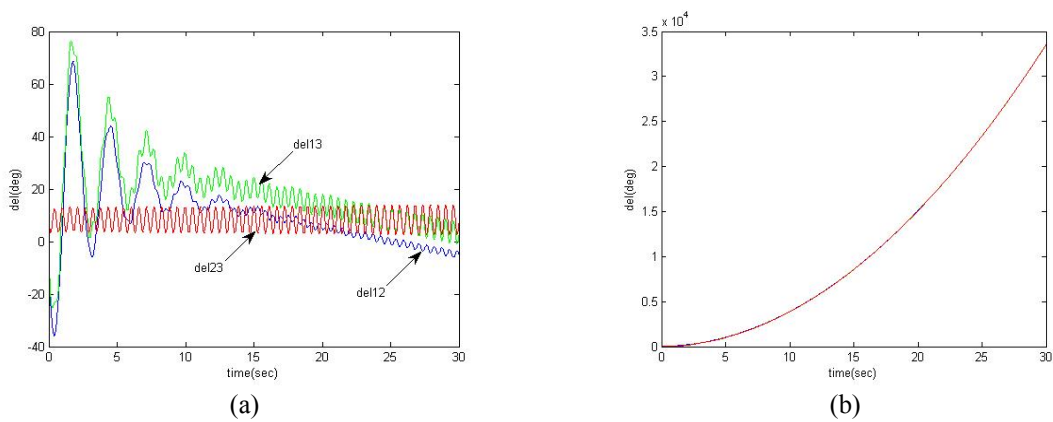


Figure 16. Plot of (a) Relative angles with ANN based PID controller (b) Absolute angles with ANN based PID controller when HVDC at 4-5 & fault at 4-6

4.3.4. Case II when HVDC at 4-5 and Fault at 8-9

From case I it is observed that among all the ANN based controller, the ANN based PID controller is good in performance. Therefore, for case II, the ANN based PID controller is preferred.

When fault occurs at line 8-9 then by using ANN based PID controller, the system gets stable and maintain the synchronism the response of relative angles δ_{23} , δ_{13} & δ_{12} obtained is plotted in figure 17(a). Also, the response of absolute angles is shown in the figure 17(b).

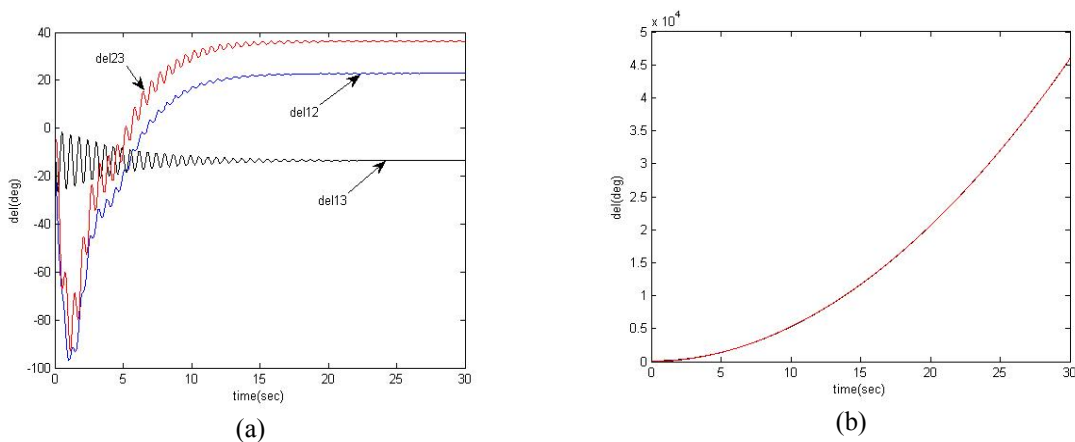


Figure 17. Plot of (a) Relative angles with ANN based PID controller (b) Absolute angles with ANN based PID controller when HVDC at 4-5 & fault at 8-9

5. CONCLUSION

The paper presents the design of a very simple form of NN-based controller. In this paper, the possibility of replacing a traditional P, PI and PID controller with a NN-based controller for the rectifier terminal of an HVDC link is explored. This NN controller is trained off-line. The NN controller has no variable characteristics of the systems inherently trained into it. Considering the HVDC current controller and line dynamics, it is observed that the transient stability of the multi-machine system is improved only if the combination of all the three signals derived from relative speed, rotor angle and average acceleration is used.

NN-based controller has been implemented successfully for HVDC power modulation to augment the transient stability. The NN-based controller gives better performance than the conventional controller when compared to the operating time of the controller. Also, among all the controllers (conventional and NN based), NN based PID controller has the better performance. However to improve the transient response of system with the off-line controller, the existing off-line controller can be trained on-line.

APPENDIX

Nine bus system data.

Table 1. Generator Data

| Generator | X_d' (pu) | H (MJ/MVA) |
|-----------|-------------|------------|
| 1 | 0.0608 | 23.64 |
| 2 | 0.1198 | 6.4 |
| 3 | 0.1813 | 3.01 |

Table 2. Transformer Data

| Transformer | X(pu) |
|-------------|--------|
| 1 | 0.0576 |
| 2 | 0.0625 |
| 3 | 0.0586 |

Table 3. Transmission Network Data

| Bus | | R(pu) | X(pu) | $y'/2'$ (pu) |
|-----|---|--------|--------|--------------|
| p | q | | | |
| 1 | 4 | 0.0 | 0.0576 | 0.0 |
| 2 | 7 | 0.0 | 0.0625 | 0.0 |
| 3 | 9 | 0.0 | 0.0586 | 0.0 |
| 4 | 6 | 0.017 | 0.092 | 0.079 |
| 5 | 7 | 0.032 | 0.161 | 0.153 |
| 6 | 9 | 0.039 | 0.17 | 0.179 |
| 7 | 8 | 0.0085 | 0.072 | 0.0745 |
| 8 | 9 | 0.0119 | 0.1008 | 0.1045 |

Table 4. DC line Data

| | | |
|-----------------------------|----------------------------|-------------------|
| $r_d = 0.017$ (pu), | $x_c = 0.6$ (pu), | $L_d = 0.05$ (pu) |
| $\alpha_{\min} = 5^\circ$, | $\alpha_{\max} = 80^\circ$ | |
| $\tau_{p\min} = 0.96$, | $\tau_{p\max} = 1.06$ | |
| $\tau_{i\min} = 0.99$, | $\tau_{i\max} = 1.09$ | |

Table 5. Bus data

| Bus no. | 1 | 2 | 3 | 4 | 5 | 6 | 7 | 8 | 9 |
|-----------|------|-------|-------|-----|------|-----|-----|------|-----|
| P_{gen} | 0.0 | 1.63 | .85 | 0.0 | 0.0 | 0.0 | 0.0 | 0.0 | 0.0 |
| P_D | 0.0 | 0.0 | 0.0 | 0.0 | 1.25 | 0.9 | 0.0 | 1.0 | 0.0 |
| Q_d | 0.0 | 0.0 | 0.0 | 0.0 | 0.5 | 0.2 | 0.0 | 0.35 | 0.0 |
| V_{sp} | 1.04 | 1.025 | 1.025 | -- | -- | -- | -- | -- | -- |

Initial Conditions

$$\begin{array}{lll}
 \alpha = 0.2094 & \text{gama} = 0.3142 & \\
 I_d = 0.3691 & P_{di} = 0.406 & V_{di} = 1.1 \\
 P_{m(1)} = 0.756646 & P_{m(2)} = 1.63 & P_{m(3)} = 0.85 \\
 \delta_{M[1]} = 2.388448^0 & \delta_{M[2]} = 18.603189^0 & \delta_{M[3]} = 12.314856^0
 \end{array}$$

Table 6. Response time of conventional and NN based Controllers

| Controll ers | Conv. PI | NN based PI | Conv. PI | NN based PI | Conv. PID | NN based PID |
|--------------------|-------------|-------------------|-------------|-------------------|--------------|--------------------|
| Operati ng time | 25 Sec. | 18 Sec. | 23 Sec. | 16 Sec. | 22 Sec. | 12 Sec. |

ACKNOWLEDGMENT

The authors would like to express their most sincere gratitude to those people, listed in the References, who in the past years have greatly contributed to the advancement of the technique applied in this paper.

REFERENCES

- [1] P Kundur. "Power System Stability and Control". McGraw- Hill, Inc., 1994.
- [2] A Ekstrom and G Liss. "A refined HVDC control system". *IEEE Trans. Power Apparatus and Systems*. vol. PAS-89, no. 536, May/June 1970.
- [3] T Smed, G Anderson, "A New Approach to AC/DC Power Flow", *IEEE Trans. on Power Systems*, Vol. 6, No. 3, pp 1238- 1244, Aug. 1991.
- [4] KR Padiyar. "HVDC Power Transmission Systems". New Age International (P) Ltd., 2004.
- [5] Stagg and El- Abiad. "Computer Methods in Power System Analysis". *International Student Edition*. McGraw- Hill, Book Company, 1968.
- [6] Garng M Huang and Vikram Krishnaswamy. "HVDC Controls for Power System Stability". *IEEE Power Engineering Society*. pp 597- 602, 2002.
- [7] VS Reddy, PVR Rao. "Supplementary HVDC Controls for Multi-machine System Stability Improvement". *IEEE (India)*. vol.89, June 2008.
- [8] VK Sood, N Kandil, RV Patel and K Khorasani. "Comparative Evaluation of Neural-Network-Based and PI Current Controllers for HVDC Transmission". *IEEE Transactions on Power Electronics*. Vol. 9, No. 3, May 1994.
- [9] B Widrow and F Smith. "Pattern recognizing control system". in Proc. Computational and Informational Sei. (COINS), Washington, Spartan, 1966.
- [10] W Miller, R Sutton, and P Werbos. "Neural Networks for Control". Cambridge, MA: MIT Press, 1991.